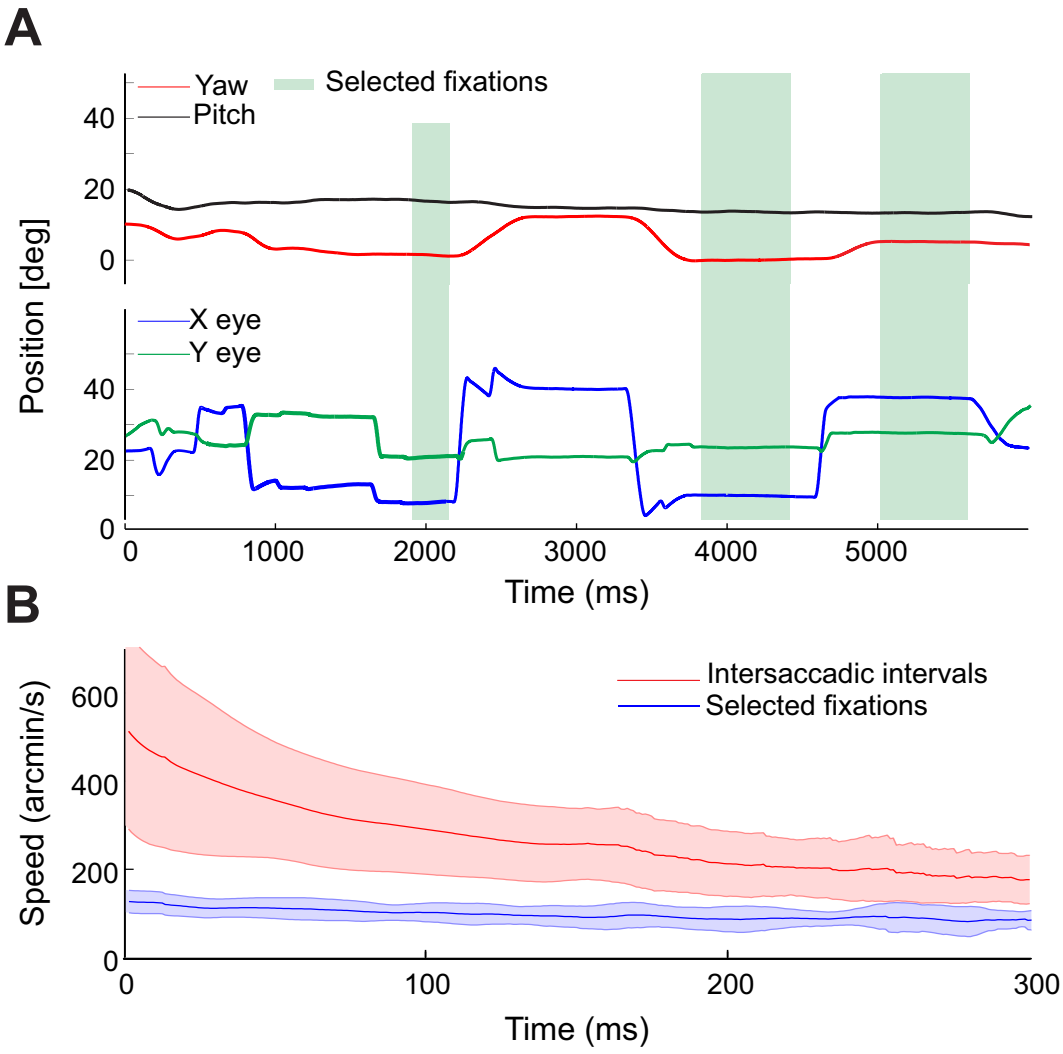

Figure S1, related to Figure 1: Selected fixations. Only very steady periods of fixation were considered in this study. (*A*) Examples of head and eye movements during an experimental trial. Shaded segments mark the periods of fixation selected for data analysis. (*B*) Mean instantaneous speed of eye movements during the first 300 ms of the intersaccadic interval (red line) and during the fixation periods selected for data analysis (blue line). Lines represents averages across subjects. Shaded regions indicate one standard deviation.

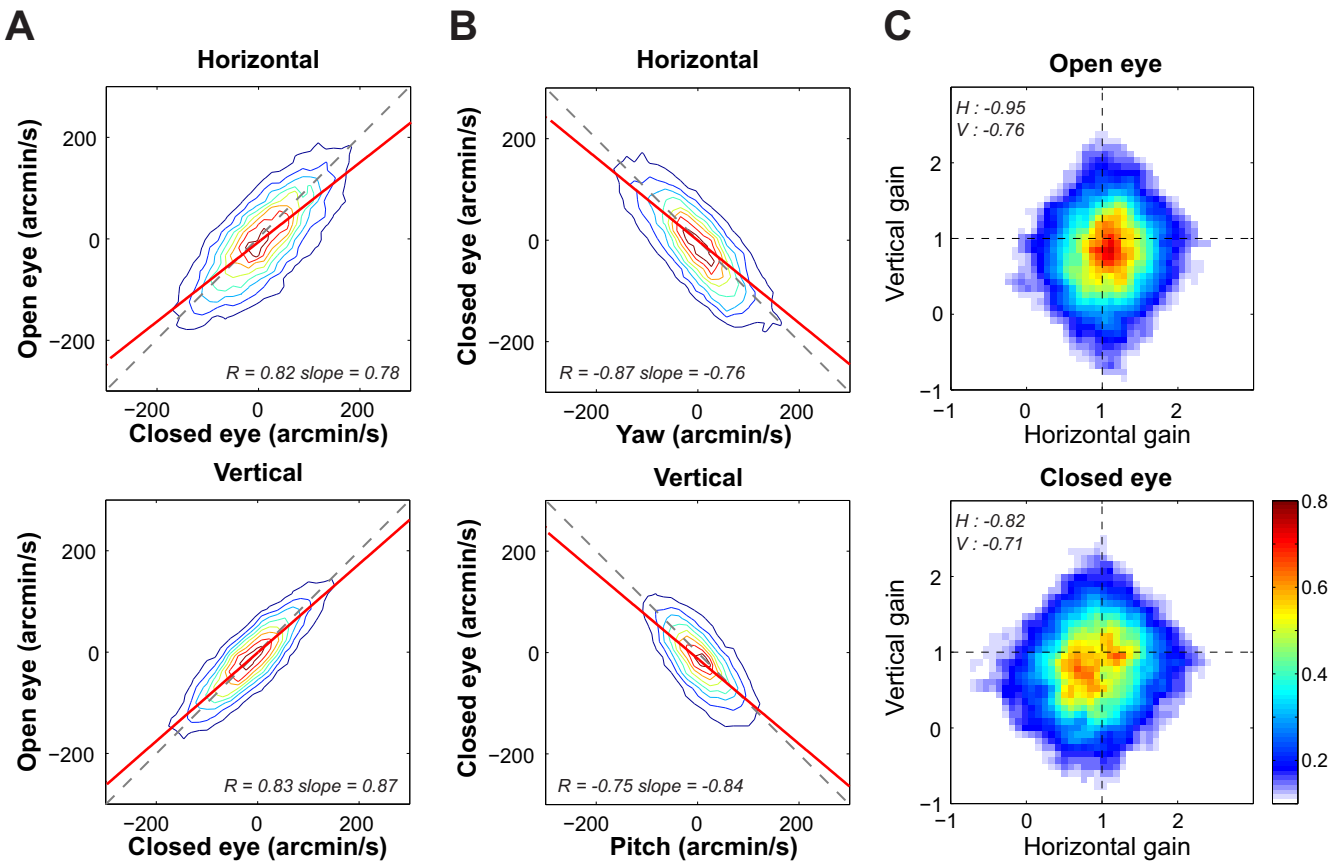

Figure S2, related to Figures 2-3: Binocular and head/eye coordination during monocular viewing. One eye was covered by an eye-patch. (*A*) Comparison between the drift velocities of the two eyes. The two rows show horizontal and vertical velocity components, respectively. (*B*) Comparison between the velocities of head and eye rotations. The horizontal and vertical components of ocular drift velocity in the covered eye are plotted as a function of the angular speeds of head yaw and pitch, respectively. Solid and dashed lines represent the linear regressions and the 45^o diagonal. (*C*) Head/eye compensation gain. Conventions are the same as in Figures 2 and 3.

Supplemental Experimental Procedures

Apparatus and procedure

In the head-free experiments, subjects wore 2D coil annuli in both eyes and a tight-fitting cap with two orthogonal coils. They were surrounded by three magnetic fields rotating at different frequencies on orthogonal planes. For each eye coil, the MRFM measures the differences between the phases of the induced currents and those in three calibrated reference coils positioned nearby the observer. It yields three angles that identify the orientation of the coil normal vector relative to the three field planes. This method has been shown to give precision higher than $1'$ even in the presence of considerable head and body motion [S1-S4]. Head rotations were measured directly from the head-coil signals and converted into yaw, pitch, and roll angles according to Fick's convention [S5]. Eye movements, the rotations of the eye within the head, were computed from both the head and eye coil signals by estimating the angles of each eye's line of sight relative to a head-centered reference frame. Head translations were measured by tracking an acoustic marker placed on the subject's head on the basis of differences in the time of arrival of the sound at four microphones. Translations were sampled at 61 Hz, a bandwidth sufficient for measuring the slow movements occurring during fixation. This methods has a resolution of $\sim$1 mm.

Calibration procedures were conducted before each experimental session to determine possible offsets in the placement of the coils, and to identify the positions of the centers of rotations of the two eyes relative to a head-centered reference frame. During this phase, the subject was positioned on a bite bar and attempted to maintain the line of sight parallel to a predefined axis with the help of an apparatus specifically designed for this purpose. The procedure was repeated for each eye, while the other eye was patched. We used the data collected during this calibration phase to estimate the level of noise in the head coils and determine the degree of binocular correlation with the head immobilized.

Subjects fixated sequentially on a series of markers. In the head-free experiments, the markers were small LEDs at 50-60 cm from the observer covering approximately $15'$. The task was performed both during normal binocular conditions and with one eye patched. In the head-fixed binocular experiment the fixation markers (crosses with $27' \times 2'$ arms) were displayed on CRT monitor at 200 Hz. In the head-fixed comparison condition of Figure $4B$, subjects freely examined natural images. In all experiments, the room was illuminated, stimuli were clearly visible, and no time constraints were imposed to the duration of fixation.

Data analysis

Selection of fixation intervals. To focus on the slow drift component of fixational eye movements, eye and head traces were filtered by a third-order Savitzky-Golay filter with cut-off frequency of approximately 30 Hz. This local polynomial regression was preferred over other low-pass filters because of its higher stability in processing the initial and final intervals of segmented traces. Similar Savitzky-Golay filters were also used for numerical differentiation to estimate velocity and acceleration.

Multiple precautions were taken to ensure selection of very steady fixation periods. We first identified saccades on the basis of the retinal trajectory of the fixated target, as the periods in which the speed of the retinal stimulus exceeded $12^o/s$. Saccade onset and offset were defined as the times at which speed became greater and lower than $4^o/s$, respectively. Inter-saccadic intervals were then processed to select periods of binocular convergence on the fixation marker. These were the intervals in which the retinal projections of the target in the two eyes (in the open eye only in the monocular experiments) remained within at least 4^o from the respective centers of gaze. Among the periods of binocular convergence, we selected the intervals in which, for both eyes, the instantaneous eye speed always remained within the 95-th percentile of the speed distribution measured at steady-state fixation, 300 ms away from saccadic events. This velocity threshold, which varied for each individual eye, was always lower than $300'$/s. We further restricted the dataset by only selecting segments longer than 150 ms and in which the overall mean speed of both eyes did not exceed $200'$/s. These criteria ensured that both the eyes and the head were in their regimes of steady fixation (see Figure S1). Fixation intervals in the head-fixed experiments were selected following the same strategy.

An average of 141 fixations (minimum 94) were selected for each subject in each of the head-free conditions. The average duration of the selected periods was of 364 ms, and the mean speed $\pm$ standard deviation of eye and head rotations were $94'$/s $\pm$ $20'$/s, and $71'$/s $\pm$ $28'$/s, respectively. These values are in the low-range of the distributions previously reported in the literature for head-free fixation [S6,S7]. Both the amplitude and length of the selected ocular drift segments were well below 1 deg. The average length, defined as the path integral along the eye trajectory, was $27'$. The average amplitude, defined as the modulus of the vector connecting the first and last point of the eye trajectory, was $17'$. In the head-fixed experiments, an average of 426 fixations (minimum 80) were selected for each subject, with average fixation duration of 342 ms. Our findings are highly robust. Very similar results were also obtained with even more stringent criteria in the selection of the fixation intervals, *e.g.*, when the speed threshold of eye speed was lowered to $200'$/s.

Correlation analysis. Levels of correlation were estimated by means of Pearson's correlation coefficients. Correlation coefficients were estimated for each subject over each selected fixation, and then averaged. All reported data represent averages across subjects.

Since the head-coil data contributed to both the estimation of head and eye rotations, the presence of noise in these data would lead to spurious correlations. We used the data collected during the preliminary calibration procedure, when subjects were immobilized by a bite-bar, to assess the extent of these noise correlations. Conservatively, we assumed that the coil signals recorded in this condition were entirely caused by noise in the system, a very conservative assumption given that small head movements continue to occur even on a bite-bar. As expected from the MRFM specifications, the power measured in this condition was smaller than 1 arcmin^2 in both head coils. Thus, the signal-to-noise ratio was over 20 during the experiments, already indicating that the influence of noise was minimal.

A very low noise impact was also confirmed by Monte Carlo simulations of the experiments, which estimated the correlation expected purely from noise. In these simulations, for each selected fixation period, we replaced the recorded head and eye coil traces with artificial time series with identical durations, and measured correlation levels using the same procedures. Each artificial trace consisted of the superposition of two terms: a noise term modeled to replicate the characteristics of the signal measured during calibration; and a Brownian process designed to model behavioral signals. The diffusion coefficient of this latter term was adjusted to make the total power in the simulated coil identical to the power measured in the experiments. To isolate spurious correlations, independent Brownian processes modeled head and eye movements. As expected, the average simulated head/eye correlation measured over 500 repetitions of the experiment was only 0.05 a value much lower than the correlation measured in the experiment ($p<0.0001$; two-tailed paired t-test). Therefore correlation values were minimally influenced by measurement noise.

Estimation of retinal image motion. The trajectory followed by the projection of the fixated target on the retina was estimated by means of Gullstrand's eye model with accommodation [S8]. This model represents the eye as a two-nodal-points optical system and the retina as a spherical surface centered at the center of rotation. The eye model was positioned in space at the estimated location of the eye's center of rotation and aligned with the measured line of sight. The positions of the rotation centers were measured during preliminary calibrations in the head-free experiments and assumed to be 13.5 mm behind the surface of the cornea in the head-fixed experiments. In the head-free experiments, the model moved following the spatial trajectories of the centers of rotations, which were estimated from the recorded head

and eye movements data. At each time step, we first computed the spatial coordinates of the fixated target within an eye-centered reference frame aligned with the line of sight, and then projected the target onto the retinal surface following the geometrical and optical constraints of the model. Note that the velocity of eye movements cannot be directly compared to the velocity of the retinal stimulus (*i.e.*, the data in Figures 1 and 4 cannot be directly compared). This happens because, although often ignored, the separation between nodal points and the center of rotation in Gullstrand's eye model introduces a magnification factor in the retinal velocity.

Supplemental References

S1. Rubens, S. M. (1945). Cube-surface coil for producing a uniform magnetic field. *Rev. Sci. Instrum.* 16, 243–245.

S2. Hartman, R. & Klinke, R. (1976). A method for measuring the angle of rotation (movements of body, head, eye in human subjects and experimental animals). *Pügers Arch. Ges. Physiol. Suppl.* 362, R52.

S3. Steinman, R. M., Kowler, E. & Collewijn, H. (1990). New directions for oculomotor research. *Vision Res.* 30, 1845–1864.

S4. Epelboim, J. et al. (1995). When push comes to shove: Compensation for passive perturbation of the head during natural gaze shifts. *Vestib. Res.* 5, 421–442.

S5. Haslwanter, T. (1995). Mathematics of three-dimensional eye rotations. *Vision Res.* 35, 1727–1739.

S6. Steinman, R. M. & Collewijn, H. (1980). Binocular retinal image motion during active head rotation. *Vision Res.* 20, 415–429.

S7. Aytekin, M. & Rucci, M. (2012). Motion parallax from microscopic head movements during visual fixation. *Vision Res.* 70, 7–17.

S8. Gullstrand, A. Appendix II. In H. von Helmholtz, J. P. C. Southall (ed.) Helmholtz's treatise on physiological optics, vol. 1, 351–352 (Rochester, NY:Dover, 1924).